

# Robust Guidewire Tracking in Fluoroscopy

Peng Wang, Terrence Chen, Ying Zhu, Wei Zhang, S. Kevin Zhou, Dorin Comaniciu  
Integrated Data Systems Department  
Siemens Corporate Research  
755 College Road East, Princeton, NJ 08540

## Abstract

A guidewire is a medical device inserted into vessels during image guided interventions for balloon inflation. During interventions, the guidewire undergoes non-rigid deformation due to patients' breathing and cardiac motions, and such 3D motions are complicated when being projected onto the 2D fluoroscopy. Furthermore, in fluoroscopy there exist severe image artifacts and other wire-like structures. All these make robust guidewire tracking challenging. To address these challenges, this paper presents a probabilistic framework for robust guidewire tracking. We first introduce a semantic guidewire model that contains three parts, including a catheter tip, a guidewire tip and a guidewire body. Measurements of different parts are integrated into a Bayesian framework as measurements of a whole guidewire for robust guidewire tracking. Moreover, for each part, two types of measurements, one from learning-based detectors and the other from online appearance models, are applied and combined. A hierarchical and multi-resolution tracking scheme is then developed based on kernel-based measurement smoothing to track guidewires effectively and efficiently in a coarse-to-fine manner. The presented framework has been validated on a test set of 47 sequences, and achieves a mean tracking error of less than 2 pixels. This demonstrates the great potential of our method for clinical applications.

## 1. Introduction

In image guided interventions, a guidewire is a medical device inserted into vessels through a guiding catheter for balloon inflation. Robust guidewire tracking is essential for many applications in image guided interventions, such as real-time assessment of guidewire position and shape, the visibility enhancement of guidewires, and guidance of co-registration between 2D and 3D imaging modalities. In this paper, we present a framework for robustly tracking a deformable guidewire in a single-view fluoroscopic sequence. Since in a clinical practice a 3D guidewire model and asso-

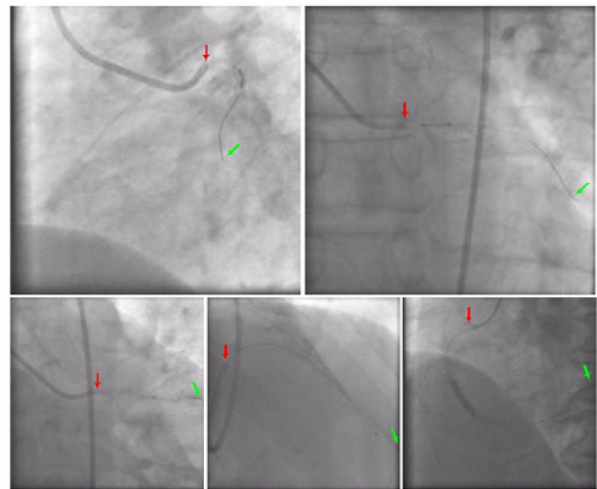


Figure 1. Some examples of guidewires in fluoroscopic sequences. The guidewires exhibit low visibility, with a variety of shapes and appearances. For better visualization, two ends of guidewires are marked with red and green arrows respectively.

ciated 3D projection matrices are not always available, our method does not rely on 3D information. Instead, the presented method is a general framework that tracks guidewire motions in 2D fluoroscopy.

Some exemplar guidewires in fluoroscopy are shown in Fig. 1. A guidewire usually starts from a tip of a guiding catheter (thicker tubes in the images), and ends at a guidewire tip. The figure demonstrates the challenges of guidewire tracking. First, guidewires are thin and with low visibility in fluoroscopic images, which usually have poor image quality due to a low dose of radiations in interventional imaging. Sometimes some segments of guidewires are barely visible in noisy images. Such weak and thin wire structures in noisy images make the robust tracking difficult. Second, guidewires exhibit large variations in their appearances, shapes and motions. The shape deformation of a guidewire is mainly due to a patient's breathing and cardiac motions in 3D, but such 3D motions become more

complicated when being projected onto a 2D image space. Third, there exist many other wire-like structures, such as guiding catheters and ribs, as shown in Fig. 1. Some of the structures are close to the guidewire, which could distract guidewire tracking and finally lead to tracking failures. All the aforementioned factors, along with robustness and speed requirements for interventions, make guidewire tracking challenging.

Due to the unique characteristics of the guidewire in fluoroscopy, conventional tracking methods would encounter difficulties and cannot deliver desired speed, accuracy and robustness for interventions. Since a guidewire is thin, the tracking methods that use regional features such as holistic intensity, textures, and color histogram [16], cannot track it well. Active contour [8, 11, 17] and level set based methods, heavily rely on intensity gradients, and are easily attracted to image noise and other wire-like structures in fluoroscopy. There is some work on guidewire detection [3] and tracking [10, 2]. Barbu et. al. [3] present a learning-based method to automatically detect guidewires in fluoroscopic sequences. The method aims at detecting a guidewire in individual frames, not continuously tracking the guidewire in a sequence. Beyar et. al. [10] use a filter based method to identify a guidewire in an X-ray image, and then use the Hough transform to fit a polynomial curve to track a guidewire. There are no quantitative reports on tracking performance in their paper. The method of Baert et. al. [2] tracks a guidewire enhanced by image subtraction and coherence diffusion. However, their experiments show that only a part of guidewire, not the whole guidewire, has been tracked.

This paper presents a probabilistic framework for robust guidewire tracking. This framework makes three contributions to address the aforementioned challenges:

1. This method introduces a semantic guidewire model, based on which a probabilistic method is presented to integrate measurements of three guidewire parts, i.e., a catheter tip, a guidewire body and a guidewire tip, in a Bayesian framework to track a whole guidewire. This tracking framework is robust to measurement noises at individual guidewire parts.
2. Robust measurement models are applied in our method to track the guidewire. Learning-based measurement models are specifically trained, from a database of guidewires, to detect guidewire parts in low-quality images. Our method further incorporates online measurement models based on guidewire appearance to improve the tracking robustness.
3. We develop a hierarchical and multi-resolution scheme to track a deforming guidewire. By decomposing the guidewire motion into two major components, the hierarchical tracking starts from a rigid alignment, followed by a refined non-rigid tracking. At each stage,

we apply a multi-resolution searching strategy by using variable bandwidths in a kernel-based measurement smoothing method, to effectively and efficiently track the deforming guidewire.

We validate the presented framework on a test set containing 47 sequences captured under real interventional scenarios. Quantitative evaluation results show that the mean tracking error on guidewires is less than 2 pixels, i.e., 0.4mm. This demonstrates the great potential of our method for clinical applications. The rest of the paper is structured as follows. We first introduce a guidewire model, and present the probabilistic formalization of guidewire tracking in Section 2.1. Details on measurement models used for guidewire tracking are provided in Section 2.2, and the hierarchical tracking scheme in Section 2.3. The quantitative evaluations of our method are presented in Section 3. Section 4 concludes the paper.

## 2. Guidewire Tracking Method

Before presenting algorithm details, we explain notations used in this paper. The regular font represents a scalar variable or function, and the bold font represents a vector, e.g.,  $\mathbf{x}$  as 2D location and  $\mathbf{u}$  as guidewire motion parameter.  $\mathbf{Z}$  is used to denote image observation, and  $\Gamma$  represents a guidewire curve.

### 2.1. Method Overview

#### 2.1.1 A guidewire model

A semantic model of a guidewire contains three parts: the catheter tip, the guidewire body, and the guidewire tip, as in Fig. 2. Each part has slightly different appearances in fluoroscopic images. For example, as shown in Fig. 1, a guiding catheter is a tube containing the guidewire, and has better visibility than the guidewire body in images. But sometimes the catheter tips can be occluded by contrast material injected during interventions. Some guidewire tips could be thicker than the guidewire body, and also show more flexible deformations. The guidewire body has the least visibility in images, but its shapes and motions are more constrained than tips.

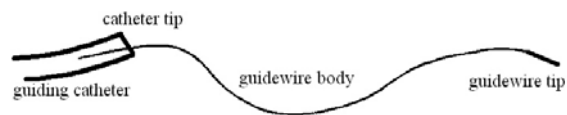


Figure 2. A semantic model of guidewire. It contains a catheter tip, guidewire body and a guidewire tip.

A spline model is used to mathematically model the guidewire. Assuming that there are  $M$  control points,  $\mathbf{x}_i^c, i = 1, \dots, M$ , on a guidewire, the guidewire can be represented as a set of points interpolated from control points,

as Eqn. (1):

$$\Gamma(\mathbf{x}) = \{\mathbf{x} = (\gamma^x(\lambda), \gamma^y(\lambda)) | 1 \leq \lambda \leq M\}, \quad (1)$$

where  $\gamma^x(\lambda)$  and  $\gamma^y(\lambda)$  are cubic spline functions, and  $\lambda \in [i-1, i]$  means that  $\mathbf{x}$  is interpolated between control points  $\mathbf{x}_{i-1}^c$  and  $\mathbf{x}_i^c$ . A general form of a cubic spline interpolation can be found in [4]. Using the spline representation, the complexity of guidewire tracking is significantly reduced. In the spline model, two controls point,  $\mathbf{x}_1^c$  and  $\mathbf{x}_M^c$ , represent the catheter tip and the guidewire tip, respectively.

### 2.1.2 A probabilistic guidewire tracking framework

Many existing tracking methods are unified in a Bayesian framework in which unknown states are inferred from sequential data [7, 16]. We also formalize the guidewire tracking in this probabilistic inference framework, to maximize the posterior probability of a tracked guidewire given fluoroscopic images. In the framework, a guidewire hypothesis at the  $t$ -th frame is a guidewire deformed from a previous frame, denoted as  $\Gamma_t(\mathbf{x}; \mathbf{u})$ :

$$\Gamma_t(\mathbf{x}; \mathbf{u}) = T(\Gamma_{t-1}(\mathbf{x}), \mathbf{u}_x), \quad (2)$$

where  $T$  is a guidewire shape transformation function, and  $\mathbf{u}_x$  is the motion parameter.  $\Gamma_{t-1}(\mathbf{x})$  is a tracked guidewire at a previous frame and is used as a template for the tracking at the  $t$ -th frame. For the simplicity of notations, a guidewire candidate is denoted as  $\Gamma_t(\mathbf{x})$ . Therefore, the posterior probability  $P(\Gamma_t(\mathbf{x})|\mathbf{Z}_t)$  is given in Eqn. (3).

$$P(\Gamma_t(\mathbf{x})|\mathbf{Z}_t) \propto P(\Gamma_t(\mathbf{x}))P(\mathbf{Z}_t|\Gamma_t(\mathbf{x})). \quad (3)$$

The tracked guidewire  $\hat{\Gamma}_t(\mathbf{x})$  is estimated as the guidewire candidate that maximizes the posterior probability, i.e.,  $\hat{\Gamma}_t(\mathbf{x}) = \underset{\Gamma_t(\mathbf{x})}{\operatorname{arg\,max}} P(\Gamma_t(\mathbf{x})|\mathbf{Z}_t)$ .

In Eqn. (3),  $P(\Gamma_t(\mathbf{x}))$  is a prior probability, which can be propagated from previous tracking results. We model the guidewire prior probability as:

$$P(\Gamma_t(\mathbf{x})) = \frac{1}{\sqrt{2\pi}\sigma_\Gamma} \exp\left(-\frac{|D(\Gamma_t(\mathbf{x}), \Gamma_{t-1}(\mathbf{x}))|^2}{2\sigma_\Gamma^2}\right), \quad (4)$$

where  $D(\Gamma_t(\mathbf{x}), \Gamma_{t-1}(\mathbf{x}))$  is the average of the shortest distances from points on a guidewire candidate  $\Gamma_t(\mathbf{x})$  to the guidewire shape template  $\Gamma_{t-1}(\mathbf{x})$ . A large kernel size  $\sigma_\Gamma$  is chosen to allow a large guidewire deformation. Another component, the likelihood measurement model  $P(\mathbf{Z}_t|\Gamma_t(\mathbf{x}))$ , plays a crucial role in achieving robust tracking results. Given a guidewire represented by  $N$  points  $\Gamma_t(\mathbf{x}) = \{\mathbf{x}_1, \mathbf{x}_2, \dots, \mathbf{x}_N\}$  that are interpolated from control points, the guidewire  $\Gamma_t(\mathbf{x})$  is in an  $N$ -dimensional space, which make the measurement model  $P(\mathbf{Z}_t|\Gamma_t(\mathbf{x}))$  difficult to represent. To simplify the model, we assume

the measurement independency among different parts along a guidewire, i.e.,  $P(\mathbf{Z}_t|\mathbf{x}_i, \Gamma_t(\mathbf{x})) = P(\mathbf{Z}_t|\mathbf{x}_i)$ . By this assumption, we can decompose the measurement model  $P(\mathbf{Z}_t|\Gamma_t(\mathbf{x}))$  into measurements at individual guidewire points, as Eqn. (5):

$$P(\mathbf{Z}_t|\Gamma_t(\mathbf{x})) = \sum_{\mathbf{x}_i} P(\mathbf{Z}_t|\mathbf{x}_i)P(\mathbf{x}_i|\Gamma_t(\mathbf{x})), \quad (5)$$

where  $P(\mathbf{Z}_t|\mathbf{x}_i)$  is the measurements at individual points on a guidewire, and  $P(\mathbf{x}_i|\Gamma_t(\mathbf{x}))$  is the weights of individual points on a guidewire. Since the two ending points at the guidewire model represent the catheter tip and the guidewire tip, respectively, the measurement model  $P(\mathbf{Z}_t|\Gamma_t(\mathbf{x}))$  is re-written as a combination of three parts of measurements in Eqn. (6):

$$P(\mathbf{Z}_t|\Gamma_t(\mathbf{x})) = \omega_1 P(\mathbf{Z}_t|\mathbf{x}_1) + \omega_N P(\mathbf{Z}_t|\mathbf{x}_N) + \frac{1 - \omega_1 - \omega_N}{N - 2} \sum_{i=2}^{N-1} P(\mathbf{Z}_t|\mathbf{x}_i), \quad (6)$$

where  $\omega_1$  and  $\omega_N$  are the weights of the catheter tip and the guidewire tip, respectively. Usually the tips have more distinguishing characteristics than the guidewire body, so they are assigned higher weights (the tip weights are empirically set between 0.05 and 0.2 in our algorithm.) All other points on a guidewire are assigned equal weights  $\frac{1 - \omega_1 - \omega_N}{N - 2}$ .

The decomposition of the measurement model  $P(\mathbf{Z}_t|\Gamma_t(\mathbf{x}))$  as the form of Eqn.(6) allows for independent measurements of different guidewire parts, while their integration on the guidewire  $\Gamma_t(\mathbf{x})$  provides a unified measurement model for the whole guidewire. The probabilistic framework provides the flexibility to track deformable guidewires, and also ensures robustness to the measurement noise at individual parts. Another advantage of this framework is its capability of introducing different types of measurement  $P(\mathbf{Z}_t|\mathbf{x}_i)$ , at individual parts, making this framework general enough to fuse multiple measurement modalities.

## 2.2. Guidewire Measurement Models

Robust measurement models  $P(\mathbf{Z}_t|\mathbf{x}_i)$  are crucial to addressing the difficulties encountered in guidewire tracking. In our method, learning-based methods are applied for robust measurements of guidewire parts. Guidewire part detectors are learned, from off-line collected training data, to model a large variety of guidewires, especially for guidewire body and guidewire tips. Another measurement modality, online measurement model based on guidewire appearance, is combined with the learning-based measurements. Such an integration can correct failures caused by one measurement modality, such as false or missing detections of learning-based measurements, and drifting of appearance-based models, therefore is able to robustly track guidewires under various environments.

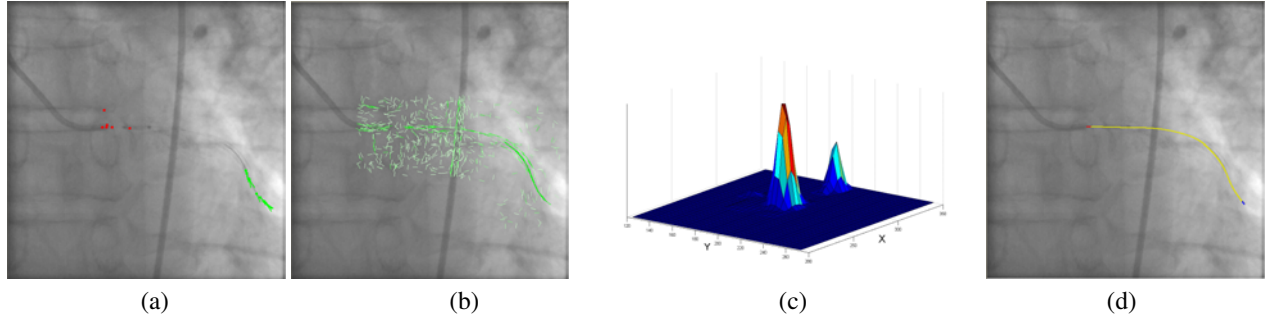


Figure 3. Guidewire measurements for robust tracking. (a): detected catheter tip candidates (red blocks) and guidewire tip candidates (green lines) in a frame; (b): the detected line segment candidates (in a region around the guidewire body) are shown in green; (c): a distribution of measurements of the catheter tip after combining learning-based and appearance-based measurements; (d): the tracked guidewire. The figures are best viewed in color.

### 2.2.1 Learning-based guidewire measurements

Learning-based detectors recently have been widely used in object detection and tracking [1, 5]. The reason behind their increasing popularity is their robustness to noises and their capability of handling objects with large variations. Different from traditional measurements based on low-level features such as edges and ridges, learning-based measurement models can be trained from a set of off-line collected data, thus being able to modeling objects with large variations. Since the training data also includes non-objects, the trained measurement models are robust to background noise. For guidewire tracking, we use the probabilistic boosting tree (PBT)[12] to construct the guidewire part detectors. PBT is a tree based general form of AdaBoost classifiers, and has a nice property of modeling a complex distribution of a class of objects. For more details on and PBT, please refer to [6, 12].

During tracking, the trained detectors can identify if an image patch at given location  $\mathbf{x}_i$  belongs to a class of objects, i.e., one of three guidewire parts in this paper. The output of an AdaBoost classifier, denoted as  $f(\mathbf{z}, \mathbf{x}_i)$ , is a combination of outputs from a collection of learned weak classifiers  $H_k(\mathbf{z}, \mathbf{x}_i)$  with associated weights  $\alpha_k$ . The numeric outputs can be further interpreted into probabilistic measurements, seeing Eqn. (7):

$$f(\mathbf{z}, \mathbf{x}_i) = \sum_k \alpha_k H_k(\mathbf{z}, \mathbf{x}_i)$$

$$P^d(\mathbf{Z}_t | \mathbf{x}_i) \propto \frac{e^{f(\mathbf{Z}_t, \mathbf{x}_i)}}{e^{-f(\mathbf{Z}_t, \mathbf{x}_i)} + e^{f(\mathbf{Z}_t, \mathbf{x}_i)}}. \quad (7)$$

In this method, we train one detector for each part of the guidewire. The guidewire body detector mainly identifies line segments of the guidewire. To train the guidewire body detector, we collect line segments from annotated guidewires as positive samples, and randomly sample the image outside guidewire as negative samples. Similarly, the guidewire tip and catheter tip detectors are trained. All the

learning-based models are built on Haar features [13], as their computational efficiency is favorable in interventional applications. Therefore, three learning-based measurement models,  $P_{cath}^d(\mathbf{Z}_t | \mathbf{x}_1)$ ,  $P_{gw}^d(\mathbf{Z}_t | \mathbf{x}_i)$ , and  $P_{tip}^d(\mathbf{Z}_t | \mathbf{x}_N)$ , are obtained for the catheter tip, guidewire body, and guidewire tip respectively. Fig. 3.(a) and (b) show the detected tip candidates and the line segment candidates of the guidewire body in a frame.

### 2.2.2 Appearance-based measurements

As shown in Fig.3, learning-based measurements may suffer from missing or false detections. This motivates us to integrate another type of measurements, appearance-based measurement, to improve the robustness of tracking. Different from the learning-based measurement model, an appearance-based measurement model aims at modeling the online appearance of a specific guidewire being tracked. In our method, the appearance-based model takes the form in Eqn. (8):

$$P^a(\mathbf{Z}_t | \mathbf{x}_i) \propto \exp\left\{-\frac{\sum_{\mathbf{x}' \in S(\mathbf{x}_i)} |\rho(\mathbf{Z}_t(\mathbf{x}') - I^0(\mathbf{x}'); \sigma_a)|^2}{2\sigma_a^2}\right\}, \quad (8)$$

where  $\mathbf{Z}_t(\mathbf{x}')$  is the image intensity at the  $t$ -th frame, and  $I^0(\mathbf{x}')$  is the corresponding image intensity at a guidewire template, which is updated from the tracked guidewire at a previous frame.  $S(\mathbf{x}_i)$  represents the geometric shape of the template, centered at the point  $\mathbf{x}_i$ . For example,  $S(\mathbf{x}_i)$  is an ellipse for the catheter tip, and a segment of guidewire for the guidewire body and tip. As defined in Eqn. (9),  $\rho$  is a robust function that is used to measure the intensity differences between current observations and the guidewire template, with removal of outliers.

$$\rho(y; \sigma_a) = \begin{cases} y, & \text{if } |y| \leq 3\sigma_a \\ 3\sigma_a, & \text{if } |y| > 3\sigma_a \end{cases}. \quad (9)$$

Similar to learning-based measurement models, we build an appearance-based model for each part of the

guidewire. So, three appearance-based measurements models,  $P_{cath}^a(\mathbf{Z}_t|\mathbf{x}_1)$ ,  $P_{gw}^a(\mathbf{Z}_t|\mathbf{x}_i)$ , and  $P_{tip}^a(\mathbf{Z}_t|\mathbf{x}_N)$ , are obtained for the catheter tip, guidewire body, and guidewire tip, respectively.

### 2.2.3 Integration of multiple measurements

The fusion of multiple measurements has been demonstrated to provide more robust tracking results than using a single measurement[15, 14]. In our method, two types of measurement models are integrated into one measurement model:

$$P(\mathbf{Z}_t|\mathbf{x}_i) = P^d(\mathbf{Z}_t|\mathbf{x}_i)P_d + P^a(\mathbf{Z}_t|\mathbf{x}_i)P_a, \quad (10)$$

where  $P_d$  and  $P_a$  are corresponding priors for two types of measurement models. Similar to the widely used mixture of Gaussians as a distribution model, Eqn. (10) explains that the  $P(\mathbf{Z}_t|\mathbf{x}_i)$  is an additive mixture model with one type of measurement model as one component. An example of integrated measurements at the catheter tip is shown in Fig. 3 (c), where the measurements have a peak at the catheter tip with false detections being suppressed.

## 2.3. Hierarchical and Multi-resolution Guidewire Tracking

The guidewire exhibits large variations in shape and motion, especially due to projections from 3D to 2D. Since a 3D guidewire model and a 3D projection matrix are not always available in a clinical practice, our method does not impose any assumptions that depends on 3D information. Instead, this method tries to handle guidewire motions that could be captured from arbitrary directions. For this purpose, our method decomposes the guidewire motion into two major steps: rigid and non-rigid motions, as the guidewire motion caused by the breathing motion can be approximated as a rigid motion in 2D, and the cardiac motion is non-rigid. The decomposed motions can be effectively and efficiently recovered in a hierarchical and coarse-to-fine manner, based on a kernel-based measurement smoothing method.

### 2.3.1 Kernel-based measurement smoothing

We here present a kernel-based measurement smoothing method for multi-resolution guidewire tracking. To obtain measurements at each point  $\mathbf{x}$  is computationally expensive, and is prone to measurement noise at individual points. For example, the measurements at points that are classified by detectors as non-guidewire parts are not reliable and ignorable in  $P^d(\mathbf{Z}_t|\mathbf{x}_i)$ . Guidewire measurements can be more robust and more efficient to compute by using kernel-based estimation (or smoothing).

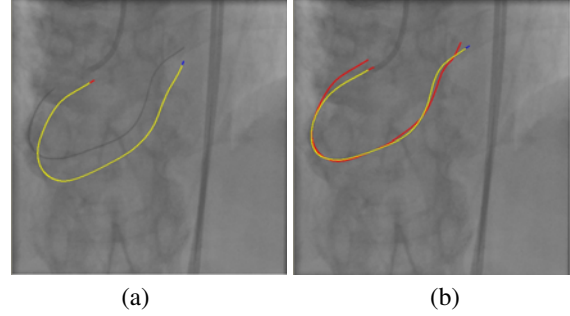


Figure 4. Hierarchical tracking. (a): tracking starts from a tracked guidewire from the previous frame (yellow line); (b): the tracked guidewire after rigid tracking (red line) and after non-rigid tracking (yellow line).

In the kernel-based estimation, measurements are made at a set of sampled locations  $\mathbf{x}_j^s$ , instead of a whole image. For learning-based measurements,  $\mathbf{x}_j^s$  are those points classified as guidewire parts, and for appearance-based measurements,  $\mathbf{x}_j^s$  are uniformly sampled points. We can conveniently assume the Markov conditional independence that the observations at sampling points  $\mathbf{x}_j^s$  are independent with the un-sampled points  $\mathbf{x}_i$ , i.e.,  $P(\mathbf{Z}_t|\mathbf{x}_i, \mathbf{x}_j^s) = P(\mathbf{Z}_t|\mathbf{x}_j^s)$ . Therefore, the kernel-based measurement estimation is represented as Eqn.(11):

$$P(\mathbf{Z}_t|\mathbf{x}_i) = \sum_j P(\mathbf{Z}_t|\mathbf{x}_j^s)G_\sigma(\mathbf{x}_j^s, \mathbf{x}_i), \quad (11)$$

where  $P(\mathbf{x}_j^s|\mathbf{x}_i) = G_\sigma(\mathbf{x}_j^s, \mathbf{x}_i)$  is a Gaussian kernel with a bandwidth  $\sigma$ . The kernel-based measurement estimation can obtain smooth measurements in a neighborhood, reduce computations of measurements, and also allow for multi-resolution searching during rigid and non-rigid tracking by varying bandwidths in kernels.

### 2.3.2 Rigid tracking

Rigid tracking aims at recovering the rigid motion of a guidewire between two successive frames. In rigid tracking, the motion parameter  $\mathbf{u}_x$  in Eqn. (2) contains only global translation and rotation, i.e.,  $\mathbf{u}_x = \mathbf{u} = (c, r, \theta)$ , where  $c, r$  and  $\theta$  are the translation and rotation parameters. Therefore, the rigid tracking is formulated as maximizing the posterior probability under a rigid motion of the guidewire, i.e., maximizing  $E(\mathbf{u})$  as below:

$$E(\mathbf{u}) = P(\Gamma_t(\mathbf{x})) \sum_{\mathbf{x}_i} P(\mathbf{x}_i|\Gamma_t(\mathbf{x}; \mathbf{u}))P(\mathbf{Z}_t|\mathbf{x}_i). \quad (12)$$

Tracking the rigid motion can be efficiently implemented using variable bandwidths in kernel-based measurement smoothing. As illustrated in Fig. 5, the rigid tracking is performed at multiple resolutions, with decreased search intervals  $\{d_1 > d_2 > \dots > d_T\}$ . During the multi-resolution

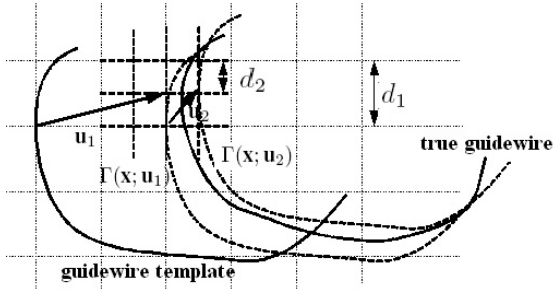


Figure 5. Multi-resolution rigid tracking with incrementally decreased search intervals and kernel bandwidths. The rigid tracking started from a template, and ends at position close to the true guidewire, up to an error caused by deformable motions. The dotted curves represent intermediate tracking results.

tracking, the corresponding bandwidth in Eqn. (11) varies accordingly, denoted as  $\sigma_i$ . At lower resolutions, we use larger kernel bandwidths to avoid missing tracking caused by larger sampling intervals; and at higher resolutions, we use smaller kernel bandwidths to obtain finer tracking results.

Furthermore, the rigid tracking is performed at both global and local scales. At a global scale, the whole guidewire is tracked, while at a local scale, a whole guidewire is divided into several local segments for rigid tracking, which follows the same formalization as Eqn.(12). By the two-stage tracking, a guidewire is roughly aligned at the current frame. A rigid tracking result is shown as the red curve in Fig. 4 (b).

### 2.3.3 Nonrigid tracking

After the rigid tracking, a guidewire is further refined by the non-rigid tracking, where the guidewire motion parameter  $\mathbf{u}_x$  is point dependent. Different from rigid deformation, the non-rigid tracking imposes a prior from guidewire smoothness constraints, as Eqn. (13):

$$E(\mathbf{u}_x) = P(\Gamma_t(\mathbf{x}; \mathbf{u}_x) | \mathbf{Z}_t) + \alpha \int \left| \frac{d\Gamma_t(\mathbf{x}; \mathbf{u}_x)}{ds} \right|^2 d\mathbf{x} + \beta \int \left| \frac{d^2\Gamma_t(\mathbf{x}; \mathbf{u}_x)}{ds^2} \right|^2 d\mathbf{x}. \quad (13)$$

The two additional terms,  $\int \left| \frac{d\Gamma_t}{ds} \right|^2 d\mathbf{x}$  and  $\int \left| \frac{d^2\Gamma_t}{ds^2} \right|^2 d\mathbf{x}$ , are integrals of the first-order and second-order derivatives of guidewire curves, and act as guidewire smoothness priors to prevent over-deformations of guidewires. The weights,  $\alpha$  and  $\beta$ , are then used to balance the smoothness constraints and probabilities scores. Such  $\alpha$  and  $\beta$  are empirically set (a typical value is between 0.05 and 0.2), but the tracking performance is not sensitive to the parameter settings as observed from our experiments. Although Eqn. (13) looks similar to the formalization in active contour based methods such as Snakes[8], they have fundamental differences.

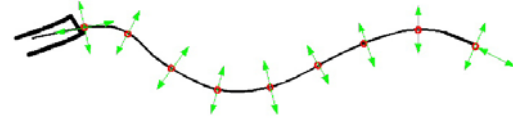


Figure 6. Non-rigid guidewire tracking. The control points (the red dots) on the guidewire body deform along normal directions, and the catheter tip and guidewire tip deform along both the normal and tangent directions.

In our method, the tracking is based on robust probabilistic measurements, while Snakes is mainly based on intensity gradients, and is prone to image noise in fluoroscopy. Our method maximizes a posterior probability, based on the novel fusion of learning-based measurements and on-line appearance measurements. Also, our method tracks an open curve of a guidewire, while Snakes and level set based methods [8, 11, 17] mainly handle closed object boundary. At last, our method integrates multiple measurements from different guidewire parts, making it more suitable to track a wire structure.

The search space of the non-rigid guidewire motion in Eqn. (13) is high dimensional. To reduce the dimensionality of the searching space, we deform control points on the guidewire body along normal directions, and two tips along both the tangent and normal directions, as illustrated in Fig. 6. But still, to exhaustively explore such a deformation space is formidable considering computational complexity. For example, if there are 20 control points, and each control point has 10 deformation candidates, the searching space contains  $10^{20}$  candidates. Instead of parallelly searching or sampling the search space, our method searches guidewire deformation sequentially. At each step, only one control point deforms to achieve a maximum  $E(\mathbf{u}_x)$ . The sequential deformation will iterate until the maximum number of iterations is reached or it converges. The same as rigid tracking, the multi-resolution searching strategy is applied during the non-rigid tracking. The sequential searching strategy in most cases leads to an optimal solution, because the rigid tracking has roughly aligned the guidewire near the true shape. An example of non-rigid tracking is shown as the yellow curve in Fig. 4 (b).

## 3. Experiments

### 3.1. Data and evaluation protocol

The tracking algorithm is evaluated on a set of 47 fluoroscopic sequences. The frame size of each sequence is 512\*512 or 600\*600, with the pixel size between 0.184 mm and 0.278 mm. There are totally more than 1000 frames in the test set. The test sequences cover a variety of interventional conditions, including low image contrast, thin guidewire, and contrast injection. Some exemplar frames

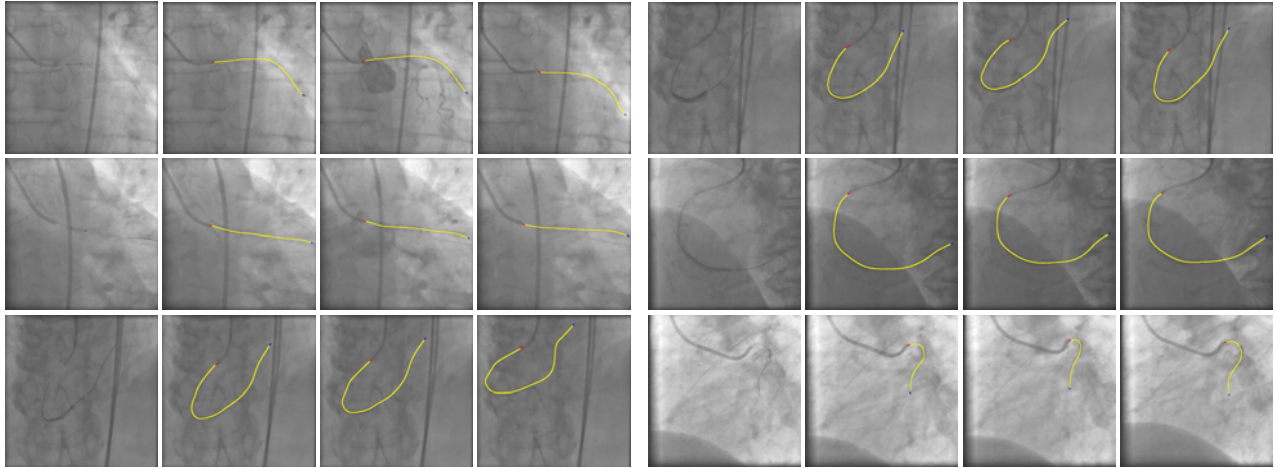


Figure 7. Some guidewire tracking results. In each graph, the left image is the first frame of a sequence, and right images show tracking results (yellow curves) at some frames. The figures are best viewed in color.

Table 1. Quantitative evaluation of guidewire (GW) tracking

Measurements models	With combined models			With only offline learned models		
	mean	std	median	mean	std	median
Overall GW Tracking Prec. (in pixels)	1.80	3.41	0.95	7.53	27.37	1.05
GW Body Tracking Prec. (in pixels)	1.70	2.96	0.95	1.79	4.02	0.97
GW Tip Tracking Prec. (in pixels)	5.45	8.21	3.69	9.06	15.43	3.79
Cath. Tip Tracking Prec. (in pixels)	11.62	12.76	7.18	68.33	76.85	35.85
GW Missing Tracking Rate	9.88%	8.43%	8.27%	11.06%	13.97%	8.55%
GW False Tracking Rate	9.62%	6.92%	7.80%	11.87%	9.74%	9.33%

in the test set are displayed in Fig. 7. The guidewire part detectors are trained on a set of 500 guidewire images that are previously collected[3].

To establish ground truth for evaluation, we manually annotate the guidewires in the test set as the ground truth. An annotated guidewire starts from a guiding catheter tip, and ends at a guidewire tip. For the purpose of evaluating tracking performance, the annotation at the first frame of each sequence is used to initialize the guidewire tracker, and the rest of annotation is used for validations. In clinical applications, the guidewire can be automatically initialized at the first frame [3], or semi-automatically detected using the interactive detection method [9].

To comprehensively and quantitatively evaluate the performance of guidewire tracking, we define a set of performance metrics, including **overall guidewire tracking precision**, **guidewire body tracking precision**, **tip tracking precision** and **missing and false tracking rate**, as follows.

1. The **overall guidewire tracking precision** is defined as the average of shortest distances from points on a tracked guidewire to the corresponding annotated guidewire. Such a precision describes how close a tracked guidewire is to the ground truth.

2. The **guidewire body tracking precision** is the tracking precision specifically at the guidewire body. The tracking errors at tips are excluded in evaluating the guidewire body tracking precision.
3. The **tip tracking precision** is the tracking precision specifically at the catheter and guidewire tips.
4. The **missing and false tracking rates** describe the percentages of guidewire points that have not been successfully tracked. A miss-tracked guidewire point is the point on an annotated guidewire whose shortest distance to the tracked guidewire is greater than a preset threshold (e.g., a threshold of 3 pixels is used in this evaluation.) A false-tracked guidewire point is the point on a tracked guidewire whose tracking error is greater than the threshold. Missing and false tracking rates are the percentages of such failed guidewire points.

### 3.2. Quantitative evaluations

Some guidewire tracking results in fluoroscopic sequences are shown in Fig. 7. Our method can successfully track the guidewire, even for those sequences with low visibility, background distraction, and contrast injection. For quantitative evaluations, the performance metrics defined in

Section 3.1, are computed on the test set. Table 1 summarizes quantitative evaluations of our tracking methods, and also compares the performance of using combined measurements with tracking only using learning-based measurements. For each performance metric, we compute its mean, standard deviation, and median. As shown in the table, the overall guidewire tracking precision is around 1.8 pixels, i.e., less than 0.4mm. The tracking errors on the guidewire and catheter tips are greater than on the guidewire body, because the motions are larger on the tips, and the background distractions affect more on tips than on the guidewire body. Our method successfully tracks more than 90% points on the guidewire, with a false tracking rate lower than 10%.

Table 1 also shows the tracking accuracy when only using learning-based measurements. It demonstrates that using both measurements improves the tracking robustness, as the mean and standard deviation of tracking errors have been reduced, especially at the catheter tip where the appearance-based measurement plays a dominant role. The large tracking errors of learning-based measurements at catheter tips are mainly caused by image noises and occlusions by contrast injection during interventions. Another important observation is that the learning-based measurements provide fairly robust measurements on the guidewire body and guidewire tips, as the improvement of tracking precision on guidewire body and tip is smaller than on the catheter tip. This confirms the advantage of our framework that unifies multiple measurements from different guidewire parts in a principled way.

The presented method is not sensitive to parameter changes. Due to limited space, we present only one experiment in Fig. 8, which shows the tracking accuracy does not change much with a wide range of a parameter  $\alpha$ , i.e., the weight of the smoothness constraint based on the first-order derivative of guidewire curves. Validations on other parameters show similar results. We conclude from the quantitative evaluations that our probabilistic tracking method provides robust and accurate guidewire tracking results. This method currently runs at 2 frames per second at a Core 2 Duo 2.0GHz computer, and can achieve a near real-time speed with an implementation optimization, such as multi-

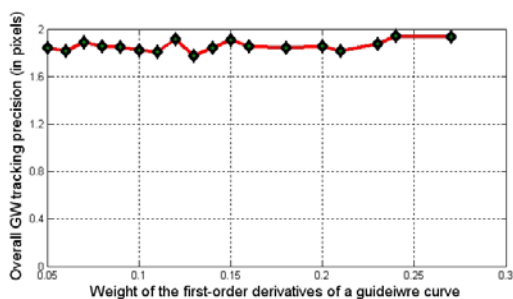


Figure 8. The tracking accuracy and an algorithm parameter (the weight of the first-order derivative of guidewire curves).

threading and GPU accelerations.

## 4. Conclusion

This paper presents a probabilistic framework of robust guidewire tracking in fluoroscopy for image guided interventions. Our framework can track non-rigid guidewire motions under arbitrary projections. The validation on a test set of 47 real interventional sequences demonstrates that this method provides robust and accurate tracking results. The future work will be integrating guidewire tracking into clinical applications, such as breathing motion compensation.

## References

- [1] S. Avidan. Ensemble tracking. *CVPR*, pages 130–136, 2005. 4
- [2] S. A. M. Baert, M. A. Viergever, and W. J. Niessen. Guide wire tracking during endovascular interventions. *IEEE Trans. Med. Imaging*, 22(8):965–972, 2003. 2
- [3] A. Barbu, V. Athitsos, B. Georgescu, S. Boehm, P. Durlak, and D. Comaniciu. Hierarchical learning of curves application to guidewire localization in fluoroscopy. In *CVPR*, 2007. 2, 7
- [4] R. H. Bartels, J. C. Beatty, and B. A. Barsky. *An Introduction to Splines for Use in Computer Graphics and Geometric Modelling*. Morgan Kaufmann, 1998. 3
- [5] G. Carneiro, B. Georgescu, S. Good, and D. Comaniciu. Detection and measurement of fetal anatomies from ultrasound images using a constrained probabilistic boosting tree. *IEEE Trans. Med. Imaging*, 27(9):1342–1355, 2008. 4
- [6] J. Friedman, T. Hastie, and R. Tibshirani. Additive logistic regression: a statistical view of boosting. *The Annals of Statistics*, 28(2):337–374, 2000. 4
- [7] M. Isard and A. Blake. CONDENSATION: conditional density propagation for visual tracking. *International Journal of Computer Vision*, 29(1):5–28, 1998. 3
- [8] M. Kass, A. Witkin, and D. Terzopoulos. Snakes: Active contour models. *International Journal of Computer Vision*, 1(4):321–331, 1987. 2, 6
- [9] P. Mazouer, T. Chen, Y. Zhu, P. Wang, P. Durlak, J.-P. Thiran, and D. Comaniciu. User-constrained guidewire localization in fluoroscopy. In *Medical Imaging: Image Processing*, Proc. SPIE, 2009. 7
- [10] D. Palti-Wasserman, A. M. Brukstein, and R. Beyar. Identifying and tracking a guide wire in the coronary arteries during angioplasty from x-ray images. *IEEE Trans. Biomedical Engineering*, 44(2):152–164, 1997. 2
- [11] L. Staib and J. Duncan. Boundary finding with parametrically deformable models. 2, 6
- [12] Z. Tu. Probabilistic boosting-tree: Learning discriminative models for classification, recognition, and clustering. In *ICCV*, pages 1589–1596, 2005. 4
- [13] P. Viola and M. Jones. Robust real-time object detection. *International Journal of Computer Vision*, 57(2):137–154, 2004. 4
- [14] P. Wang and Q. Ji. Robust face tracking via collaboration of generic and specific models. *IEEE Trans. on Image Processing*, 17(7):1189–1199, July 2008. 5
- [15] Y. Wu and T. S. Huang. Robust visual tracking by integrating multiple cues based on co-inference learning. *International Journal of Computer Vision*, 58(1):55–71, June 2004. 5
- [16] A. Yilmaz, O. Javed, and M. Shah. Object tracking: A survey. *ACM Comput. Surv.*, 38(4):13, 2006. 2, 3
- [17] S. C. Zhu and A. L. Yuille. Forms: A flexible object recognition and modeling system. *International Journal of Computer Vision*, 20:187–212, 1996. 2, 6